

**Computational investigation on natural quinazoline alkaloids as potential inhibitors of the main protease (M<sup>pro</sup>) of SARS\_CoV\_2**

Abhisek Jana<sup>1</sup>, Tarun Roy<sup>1</sup>, Sarbajit Layek<sup>1</sup>, Subhas Ghosal<sup>1</sup>, Deb Ranjan Banerjee<sup>1\*</sup>

<sup>1</sup> Department of Chemistry, National Institute of technology Durgapur, MG Avenue, Durgapur, India-713209

\*Corresponding author; email ID: [debranjana.banerjee@ch.nitdgp.ac.in](mailto:debranjana.banerjee@ch.nitdgp.ac.in); full postal address: Deb Ranjan Banerjee, Assistant Professor, Department of Chemistry, National Institute of technology Durgapur, MG Avenue, Durgapur, India-713209

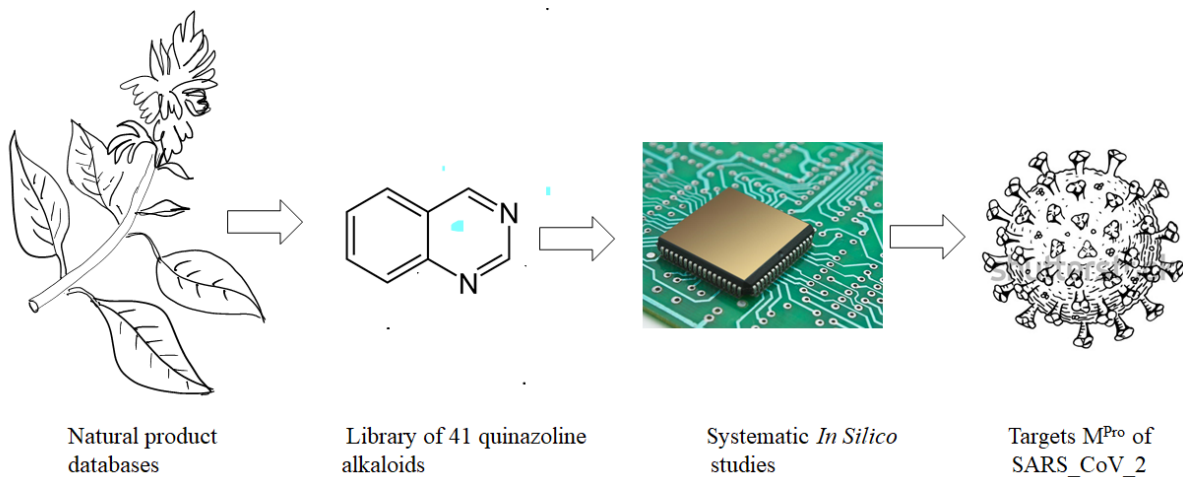
## Key words

SARS\_CoV\_2, Main Protease, Quinazoline alkaloid, In silico

## Abstract

Drug discovery is still behind in the race compared to vaccine discovery in fighting COVID-19. Recently, a few alkaloids from a traditional Indian medicinal plant, Vasaka (*Justicia adhatoda*), have been linked computationally to the main protease ( $M^{pro}$ ) of SARS\_CoV\_2. To expand the knowledge and for further investigation, we have selected 41 quinazoline alkaloids from two natural product databases to create an adequate library and performed detailed computational studies against the main protease ( $M^{pro}$ ) of SARS\_CoV\_2. The screening of the library was carried out through blending the rigid docking and pharmacokinetic analysis that resulted in nine alkaloids as initial leads against  $M^{pro}$ . These nine alkaloids were further subjected to advance flexible docking using first reference famotidine for the analysis of structure-based interactions. For further selection, a second screening was carried out based on binding energies and interaction profiles that yielded three alkaloids namely CNP0416047, 3-hydroxy anisotine and anisotine as hits. The stereo-electronic features of hit alkaloids were further investigated through additional structure-based E-pharmacophore mapping against a second reference, known X77 ligand. Additionally, the reactivity of hit alkaloids at the binding site of the protein was estimated by measuring the electron distribution on the frontier molecular orbitals and HOMO-LUMO band energies. Finally, the stabilities of complexes between hit alkaloids with the protein were accessed extensively using robust molecular dynamics simulation through RMSD, RMSF, Rg, and MM-PBSA calculation. Thus, this study identifies three natural quinazoline alkaloids as potential inhibitors of  $M^{pro}$  through extensive computational analysis.

## Graphical Abstract



## 1.0. Introduction:

The discoveries made by scientists across the globe unmasked a number of protein targets and pathways to defeat SARS\_CoV\_2 which is the causative agent behind COVID19 (1, 2). Many of these targets have been explored for drug repurposing, but the discovery of a specific drug against a specific target of SARS\_CoV\_2 is still at large. The main protease ( $M^{Pro}$ ) of SARS\_CoV\_2 is one such potential target due to its' essential role in processing the polyproteins that are translated from viral genomic RNA during the viral replication inside the host cell (3, 4, 5). As the processing of polyproteins is absolutely essential for the replication of the virus, hence it's possible to prevent COVID-19 progression in the host by inhibiting the main protease ( $M^{Pro}$ ). The solved crystal structure of  $M^{Pro}$  (6) paved the platform for the computational validation and identification of new leads against the main protease of the virus causing COVID-19 which is still an ongoing global emergency. Importantly, the absence of any human protease with a similar cleaving profile as  $M^{Pro}$  rules out the possibility of off-target effects of its inhibitor. Therefore,  $M^{Pro}$  is being targeted for drug repurposing and virtual screening (7, 8, 9, 10) in recent times.

On the other hand, natural product libraries always act as an excellent pool to find therapeutic agents against a new biological target (11). The availability of diverse natural compound databases and recent advances in computational chemistry have made the screening of potential inhibitors easier, but surely attention should be given towards the structure-based means and sample number to remove the promiscuities. Nevertheless, natural compounds from traditional Indian medicinal trees such as Vasaka tree (*Justicia adhatoda*) and Neem tree (*Azadirachta indica*) have been scientifically proven to have bronchodilatory and respiratory stimulants (12, 13). Importantly, one major alkaloid found in Vasaka leaves is Vasicine that is linked with inhibition of proteases enzyme isolated from *Pseudomonas aeruginosa* (13). Therefore, natural compounds from these sources have been targeted for early-phase screening against SARS\_CoV\_2 proteins. For example, computational screening of natural compounds from Neem tree against SARS\_CoV\_2 M and E proteins have been reported in the search to find potential hits (14). Additionally, phytochemicals from traditional Indian medicinal plants such as *Justicia adhatoda*, *Ocimum sanctum* and *Swertia chirata* have been computationally screened against two SARS\_CoV\_2 proteins, namely the protease enzyme ( $M^{Pro}$ ) and RNA-dependent RNA polymerase (RdRp) (15). In this study, an alkaloid named anisotine was reported as a dual inhibitor of both proteins, whereas a polyphenol named Amarogentin was reported as best inhibitor of RdRp. However, crucial structure-based information was not provided in this report in support of promiscuous inhibition profiles exhibited by structurally different inhibitor molecules against two totally different protein targets. Additionally, an *in silico* attempt has been reported to find inhibitors of main protease ( $M^{Pro}$ ) by taking only six alkaloids from Vasaka tree (16).

In this study, we have done a detailed computational investigation on natural quinazoline alkaloids by constructing an adequate library of 41 samples from two natural product databases in the search for potential inhibitors of the main protease ( $M^{Pro}$ ) of SARS\_CoV\_2. After two rounds of screenings based on rigid docking, flexible docking and ADMET profiling, we identified three quinazoline alkaloids as promising hit compounds. Furthermore, the stereo-electronic features of hit alkaloids were further investigated through additional structure-based E-pharmacophore mapping and DFT based calculations. Finally, the stabilities of complexes between hit alkaloids with the protein were accessed extensively using robust molecular dynamics simulation through RMSD, RMSF, Rg, and MM-PBSA calculation.

## 2.0. Materials and Methods:

**2.1. Preparation of protein and ligand structures:** The high-resolution X-ray crystal structure of the protein (M<sup>Pro</sup>) was retrieved from RCSB PDB bank (PDB ID: 6LU7) and crystal structure was analyzed as required for the measurement of cavity size/distances/charge/shape for the structure-based drug discovery. The PyMol molecular visualization system and BIOVIA Discovery Studio Client were utilized for protein structure visualization, structure alignment and for the measurement of the distance between residues and the diameter of cavity size. The protein structure was further edited and refined as required for the docking and simulation protocol as mentioned in the specific sections. The structure of the ligand molecules was obtained from COCONUT (Collection of natural product database) (17) and NPBS (Natural product and biological source) (18). At first, the structures were drawn in ChemDraw ultra 12.0 and then Geometry optimization of the alkaloid molecules was carried out using DFT at the B3LYP (1,2) /6-31+G(d,p) level of theory in Gaussian suite of program (19, 20, 21). The geometry optimized ligand structures were subjected to refinement as required for docking as mentioned in the specific sections.

**2.2. Combined screening protocol based on rigid docking and pharmacokinetic analysis:** For rigid docking, advanced and widely used molecular grid-based docking program Autodock4.2 (22) was executed for screening purposes. Prior to docking, protein structure was edited by adding hydrogen atoms and gasteiger charges in autodocktools to create PDBQT files. The energy minimized ligand structures were further edited in autodocktools (ADT) by defining root center, aromatic carbons, and torsions. In grid selections, the whole receptor structure was selected for autogrid calculation with 0.375 Å spacing surrounding all possible binding sites to perform blind docking. Finally, docking studies were carried out using the Lamarckian Genetic Algorithm (LGA) based on the grid maps of all atoms present in the receptors and ligands. Parameters were set to an initial population of 150 randomly placed individuals, a maximum of  $2.5 \times 10^7$  energy evaluations, cluster tolerance of 2 Å (rms), output level 0 and maximum generations of  $2.7 \times 10^4$  numbers for total 10 numbers of conformations. After each docking execution, the 10 docked conformers were clustered by autodocktools based on thermodynamic parameters. The compounds exhibiting negative binding energy  $\geq 9.8$  Kcal / mol were chosen from this screening.

Total nine alkaloids, selected from rigid docking, were subjected for the evaluation of pharmacokinetic features and toxicity features using SwissADME server (23), pkCSM-pharmacokinetics server (24), and BIOVIA Discovery Studio ADMET descriptor (25). The ADME properties of the compounds were measured on SwissADME based on Lipinski's rule, and were further checked using BIOVIA Discovery Studio ADMET predictors. The possible toxicities of these compounds were estimated by pkCSM-pharmacokinetics tool. The final screening was carried out based on ADME features, non-carcinogenic features and cut-off binding energy.

## 2.3. Flexible Docking of the screened compounds for structure-based assessment of binding

Flexible docking between SARS\_CoV\_2 M<sup>Pro</sup> with screened alkaloids and reference compound famotidine were performed using CDOCKER program of BIOVIA Discovery studio (25) for detailed structure-based assessment of binding. The retrieved protein structure from RCSB database was initially subjected to 'clean protein' protocol to eradicate alternate conformations, and any error in bond order and amino acid sequence. Thereafter, the protein was further subjected to protonation at pH 7.4 and ionic strength 0.145 (M) respectively. In addition, the CHARMM force field was applied *in vacuo* for the global energy minimization of the protein structure. For the targeted docking to the active site of the protein, site sphere was created with co-ordinates set to -12.0702, 13.4652, and 68.368 respectively.

Finally, the CDOCKER program was executed with customized parameters where the pose cluster radius was set to 0.5, total random conformations were set to 10, total dynamics steps were set to 1000. Additionally, in the simulated annealing section heating steps and target temperature were set to 2000 and 700 K simultaneously, cooling steps and target temperature was 5000 and 300 K simultaneously. After each docking, ten docking conformers were ranked automatically based on –CDOCKER energy, and evaluated further for molecular-level analysis of the bindings.

**2.4. HOMO-LUMO measurement by density functional theory calculation:** The geometry of the alkaloid molecules were optimized in gas phase using B3LYP functional as implemented in Gaussian 09 software (26) using the 6-311+G(d,p) basis set. The geometry optimization of the molecules was also done using another hybrid density functional with empirical dispersion correction ( $\omega$ B97XD) (27) with same basis set for verification. The energies of the Highest Occupied Molecular Orbital (HOMO) and Lowest Unoccupied Molecular Orbital (LUMO) and the electron density distributions of these frontier orbitals were captured by using GAUSS-VIEW software. The HOMO-LUMO energy gap has been linked to reactivity of a molecule and extrapolated to the activity of the bound inhibitor inside the enzyme catalytic cavity (28).

**2.5. E-pharmacophore modeling:** E-pharmacophore model was built using the recently published co-crystal structure of X77 inhibitor with protein M<sup>Pro</sup> (PDB ID 6W63). For this purpose, the co-crystal structure was retrieved from RCSB database, then ‘interactive pharmacophore model’ was generated in BIOVIA Discovery studio by selecting the protein as receptor and the X77 inhibitor as ligand. The protocol was set to calculate maximum ten pharmacophores with maximum features 6 at minimum inter-feature distance 2 with steric volume excluded for all types of non-bond interactions. The vacant E-pharmacophore was then mapped with the energy-optimized structures of selected alkaloids based on the common features. Prior to mapping, alkaloids were structurally optimized using CHARMM force field with Momary-Rone partial charge at pH 7.4 and all possible tautomers, stereoisomers and protonation states were generated.

**2.6. Molecular Dynamics Simulation:** All the molecular dynamics simulations were performed using standard dynamics cascade protocol of BIOVIA Discovery studio. The top docked poses of all the M<sup>Pro</sup>-inhibitor complexes were further edited by protonating at pH 7.4 at dielectric constant of 10 and subjected to CHARMM36 force field. Each system was placed in the centre of the orthorhombic simulation box modeled by the explicit periodic boundary solvation model. A minimum distance from the edge of the box was set to 7 Å and 0.145 (M) NaCl was added to each of the systems. The protein only (M<sup>Pro</sup>), protein-reference complex (M<sup>Pro</sup> –famotidine), and three final protein-inhibitor complexes (M<sup>Pro</sup> -CNP0416047, M<sup>Pro</sup> -3-hydroxyanisotine, M<sup>Pro</sup> –anisotine) were solvated with 6358, 6335, 6332, 6313, 6325 no of water molecules in the orthorhombic simulation box. All the solvated systems were minimized in two stages to sort out poor contacts within the system and to warrant the systems to gain a low energy point as required for the successive stages. Then the solvated systems were subjected to 2000 steps of the steepest descent algorithm in the first step followed by the 5000 steps of the conjugate gradient. Additionally, each of the minimized systems was slowly heated from 50 K to 300 K at a time period of 120 ns. Then the systems were equilibrated for 1 ns at a constant temperature of 300 K. In both the heating and equilibration steps, the adjusted velocity frequency was set to 50. The production step was performed for 20 ns for each of the systems using NVT ensemble at 300 K. The results of the production steps were saved after every 2 ps. During the simulation, the non-bond higher cut-off distance and lower cut-off distance were kept at 12 Å and 10 Å respectively, and the spherical cut-off method was used for the electrostatics calculation.

**2.7. Molecular mechanics-Poisson-Boltzmann surface area (MM PBSA) method:** To calculate the free energy of binding and to score the inhibitors based on it, the molecular mechanics-Poisson-Boltzmann surface area (MM PBSA) method was carried out after simulation using the BIOVIA Discovery studio. Purposefully, the trajectories of the simulations were processed before the MM PBSA calculation and the trajectories of last 5 ns simulation data with frame increment of 250 was chosen for MM PBSA calculation. The MM PBSA calculation of free energy of binding is a slowest solvent approximation method based on continuum electrostatics and a summation of the calculation of potential energy, polar and non-polar solvation energy components and depends on the free energy of complex, ligand, and receptor as following as (29, 30):

$$\Delta G_{\text{bind}} = \Delta G_{\text{complex}} - (\Delta G_{\text{receptor}} + \Delta G_{\text{ligand}})$$

### 3.0. Results and Discussion:

**3.1. Analysis of the target:** The main protease ( $M^{\text{Pro}}$ ) of SARS\_CoV\_2 virus is involved in the processing of non-structured polyproteins and essential for viral replication within the host cell (1, 2, 3). The published crystal structure of  $M^{\text{Pro}}$  (PDB ID 6LU7) has paved the road for the structure-based design of inhibitors (6) and we analyzed the crystal structure with the same purpose. The  $M^{\text{Pro}}$  crystallized as a homodimer of two protomers, where each protomer consists of 306 amino acid residues and divided into three domains: Domain I (amino acids 8 – 101), Domain II (amino acids 102 – 184) and Domain III (amino acids 201 – 303) (**Figure 1**). Additionally, each Domain II and III are connected by a Loop (amino acids 185 – 200) that is crucial for the enzymatic action of main proteases (6). The substrate-binding site and catalytic dyad (Cys145, His41) is located at a cleft between Domain I and Domain II. Furthermore, the substrate binding site is divided into four sub-sites: S1 located nearby Cys145, S1' located nearby His41, S2 located nearby hydrophobic residues namely Tyr54, and S4 located nearby the Loop region. Moreover, we have selected famotidine as one of the reference compounds as it's linked to  $M^{\text{Pro}}$  inhibition computationally (31, 32, 33, 34) and also implicated to SARS\_CoV\_2 growth inhibition (35). Additionally, we have chosen X77 molecule as a second reference in E-pharmacophore modeling as X77 is a non-covalent inhibitor and the co-crystal structure of X77-  $M^{\text{Pro}}$  is available (PDB ID 6W63) (36, 37).

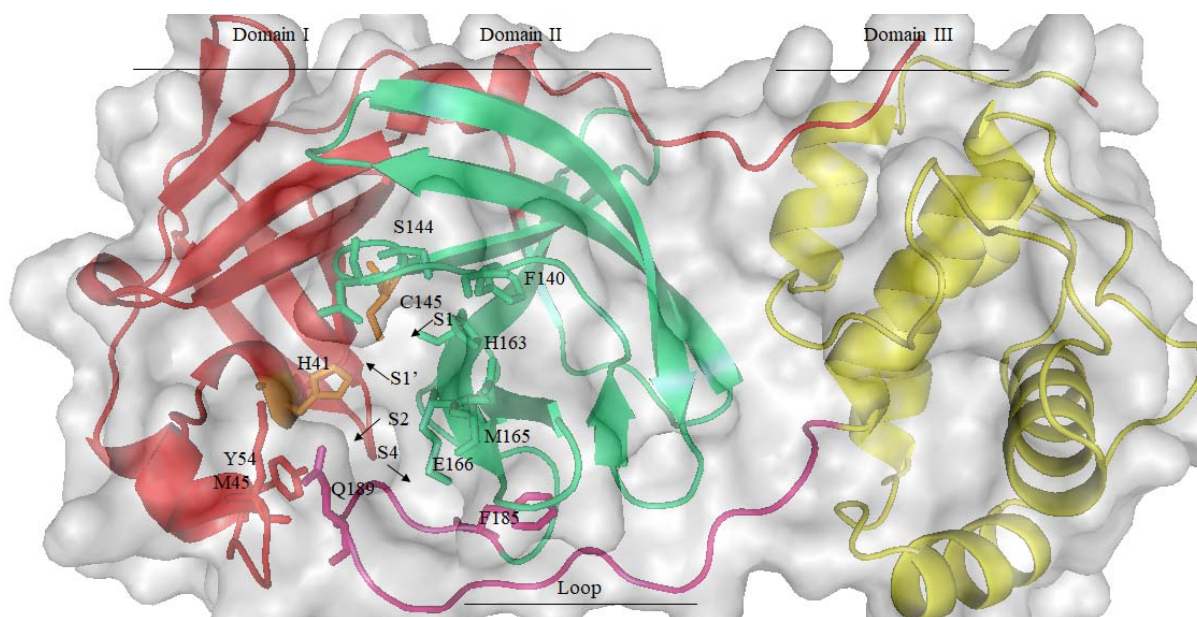
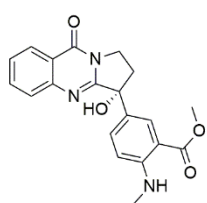
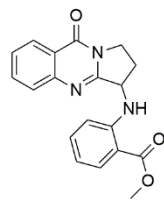


**Figure 1:** The X-ray crystal structure (PDB ID 6LU7) of the main protease ( $M^{Pro}$ ) of SARS\_CoV\_2, the protein is displayed as cartoon diagram showing the domain I (in red color), domain II (in green color), domain III (in yellow color), and loop (in magenta color). The active site cavity remains at the cleft between domain I and II, the catalytic dyad (Cys145 and His41) are displayed in orange color, the other crucial residues namely Met45, Tyr54, Phe140, His163, Met165, Asp166, Phe185, and Glu189 are shown as sticks. The subsites (S1, S1', S2, S4) are shown by arrow marks.

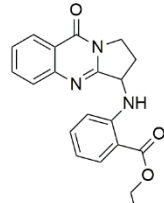
**3.2. Screening of library:** Inspired by the initial reports of natural compounds showing promising results against  $M^{Pro}$  (15, 16), we designed a computational strategy for the detailed investigation of quinazoline pharmacophore against the main protease of SARS\_CoV\_2. Purposefully, we constructed an adequate library of 41 natural quinazoline alkaloids (**Figure 2**) from two natural product databases, COCONUT (17) and NPBS (18), for a full-scale investigation. The initial screening of 41 compounds against our target  $M^{Pro}$  was a necessary task and achieved by blending rigid molecular docking and pharmacokinetic analysis (**Figure 3**). In brief, the entire library of compounds along with reference famotidine was subjected to grid-based rigid docking by Autodock4.2 using blind docking protocol where the entire protein was selected in grid mapping covering all possible binding sites. It was observed that all the alkaloids bind at the substrate binding cavity of the main protease and interact with the loop crucial for the enzymatic mechanism of the target (6). Comparing the binding energy and inhibition constant found from docking studies, we observed that alkaloids having an aromatic moiety at C3 of tetrahydropyrrole ring and at C6 of quinazoline frame displayed better result. For the screening purpose, the alkaloids were ranked according to their negative binding energy as obtained from the rigid docking as shown in **Table 1**. An initial cut-off was employed and nine compounds were selected having negative binding energy  $\geq 9.8$  Kcal/mol for the second screening based on pharmacokinetic analysis. These nine compounds were further evaluated for their pharmacokinetic and toxicity features using SwissADME server (23), pkCSM-pharmacokinetics server (24), and BIOVIA Discovery Studio ADMET predictors (25). The ADME properties of the compounds were measured on SwissADME based on Lipinski's rule (**Supporting Table 1**), and were further checked using BIOVIA Discovery Studio ADMET predictors (**Supporting Figure 1**). Additionally, the possible toxicities of these compounds were estimated by pkCSM-pharmacokinetics tool. The molecular weight of all the quinazoline alkaloids ranges between 335.36 to 427.45 indicating the efficient absorption, transportation and diffusion in the body. Moreover, the TPSA values of the 9 alkaloids were found to be in the range between the 70 - 90  $\text{\AA}^2$  indicating good intestinal absorption and cell permeability. Overall, the initial screened alkaloids showed good bio-availabilities based on Lipinski's rule and toxicity prediction.



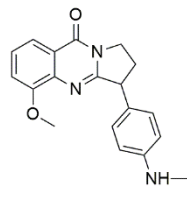
3-Hydroxy anisotine



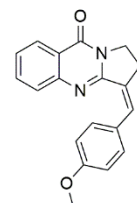
Vasnetine



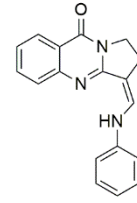
Annisessine



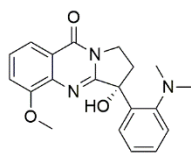
CNP0300419



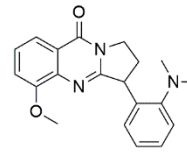
CNP0363970



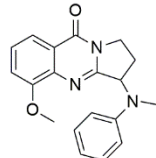
CNP0362429



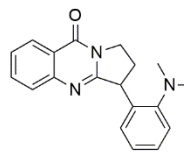
Aniflorine



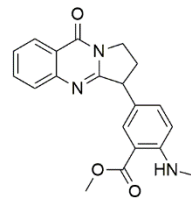
Deoxy-aniflorine



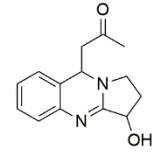
Sessiflorine



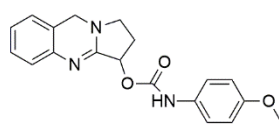
Vasicoline



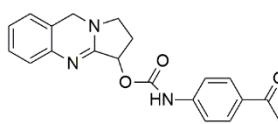
Adhatodine



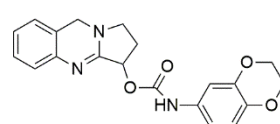
CNP0231441



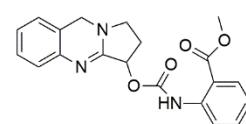
CNP0231874



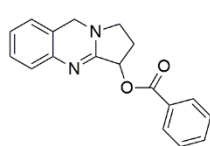
CNP0292663



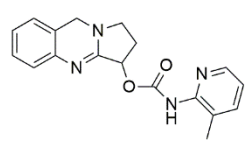
CNP0368475



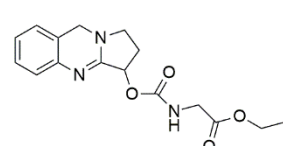
CNP0368540



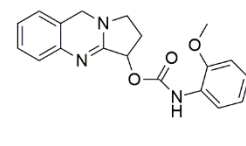
CNP0366885



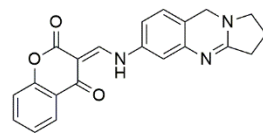
CNP0389911



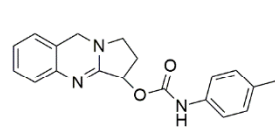
CNP0368589



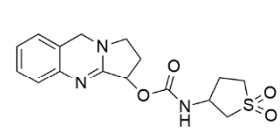
CNP0294473



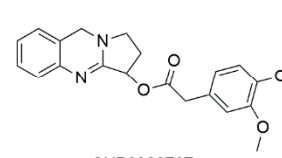
CNP0297469



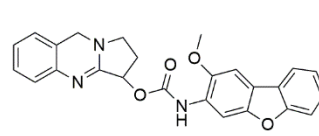
CNP0382594



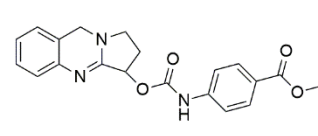
CNP0378904



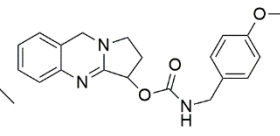
CNP0380707



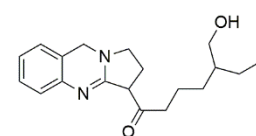
CNP0368366



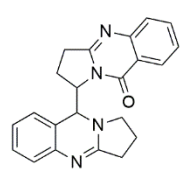
CNP0368723



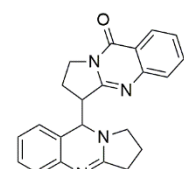
CNP0113654



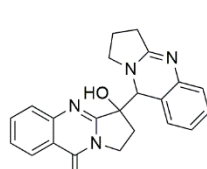
CNP0214380



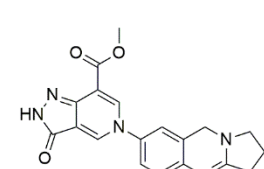
CNP0271254



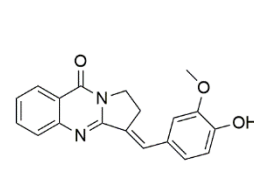
CNP0425191



CNP0102583



CNP0281399



CNP0336764

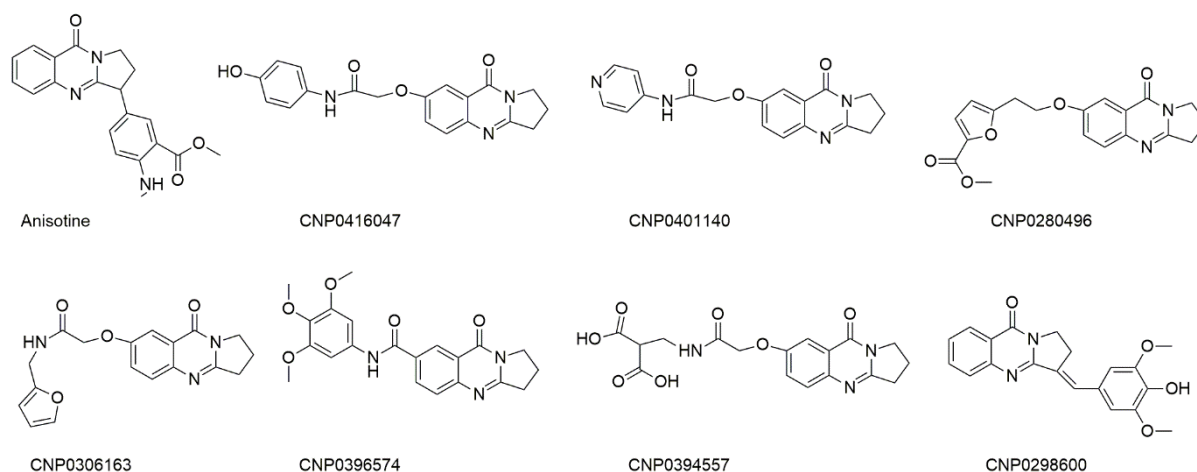


**Figure 2:** Constructed library of 41 natural quinazoline alkaloids from natural product databases COCONUT and NPBS

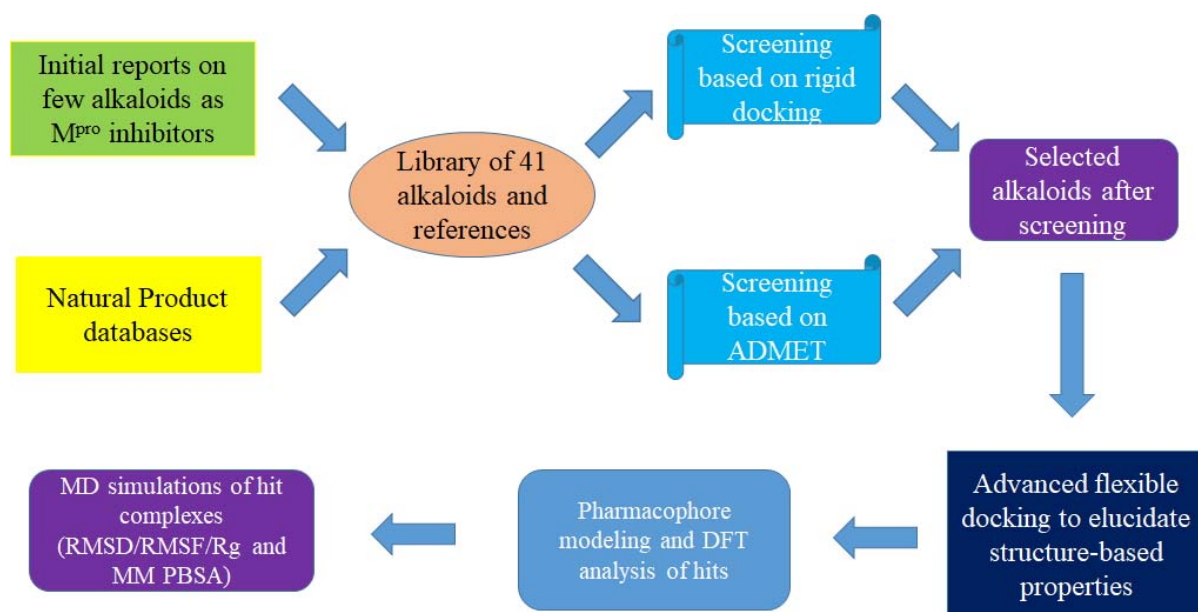


**Figure 3:** Schematic representation of our strategy on systematic investigation of quinazoline alkaloids against the main protease ( $M^{Pro}$ ) of SARS\_CoV\_2.

**Table 1:** Results of rigid docking of quinazoline alkaloids as part of screening method with their binding energies. The nine alkaloids with negative binding energies  $\geq 9.8$  Kcal/mole are shown in bold fonts.

Sr. No	Compound	(-) Binding Energy (kcal/mol)	Sr. No	Compound	(-) Binding Energy (kcal/mol)
<b>1</b>	<b>Famotidine</b>	<b>10.70</b>	22	CNP0389911	9.51
<b>2</b>	<b>CNP0368366</b>	<b>11.96</b>	23	CNP0368589	9.19
<b>3</b>	<b>CNP0416047</b>	<b>11.03</b>	24	CNP0294473	9.54
<b>4</b>	<b>3-hydroxy anisotine</b>	<b>10.99</b>	<b>25</b>	<b>CNP0297469</b>	<b>10.20</b>
<b>5</b>	<b>Anisotine</b>	<b>10.81</b>	26	CNP0382594	9.34
<b>6</b>	<b>Vasnetine</b>	<b>9.80</b>	27	CNP0378904	9.32
<b>7</b>	<b>Annisessine</b>	<b>10.20</b>	28	CNP0380707	9.75
8	CNP0300419	9.32	29	CNP0368723	9.18
9	CNP0363970	9.43	30	CNP0113654	8.77
10	CNP0362429	9.31	31	CNP0214380	7.07
11	Aniflorine	8.62	32	CNP0271254	9.20
12	Deoxy Aniflorine	8.36	33	CNP0425191	9.00
13	Sessiflorine	9.39	34	CNP0102583	9.77
14	Vasicoline	8.81	<b>35</b>	<b>CNP0281399</b>	<b>10.21</b>
15	Adhatodine	9.46	36	CNP0336764	9.58
16	CNP0231441	7.91	37	CNP0401140	9.39
17	CNP0231874	9.42	38	CNP0280496	9.26
18	CNP0292663	9.20	39	CNP0306163	9.24
<b>19</b>	<b>CNP0368475</b>	<b>10.75</b>	40	CNP0396574	9.14
20	CNP0368540	9.59	41	CNP0394557	8.89
21	CNP0366885	8.96	42	CNP0298600	8.52

**3.3. Advanced flexible docking to establish the structure based interactions:** The initially selected nine alkaloids from the screening were further subjected to the advanced flexible docking against SARS\_CoV\_2 M<sup>Pro</sup> along with the reference famotidine to assess the structure based interactions. Purposefully, the CDOCKER program of BIOVIA Discovery studio (25) equipped with flexible docking at variable temperatures using CHARMM based energy function was utilized for the detailed structure-based assessment of binding. As these alkaloids were found to be catalytic cavity binders in rigid docking as shown in screening section, therefore the flexible dockings were carried out inside the active site cavity sphere encompassing all subsites and crucial residues. The alkaloids were docked separately using customized protocol as described in materials and method section, and were ranked according to their best negative CDOCKER Interaction energies as shown in **Table 2**.

**Table 2:** The results of flexible docking in terms of interaction energies of reference compound and initially selected nine selected alkaloids

Sr No	Compound	-CDOCKER interaction energy (kcal/mol)
1	Famotidine	42.3865
2	CNP0368366	44.6628
3	CNP0416047	43.2474
4	3-hydroxy anisotine	42.4530
5	Anisotine	41.8961
6	CNP0368475	40.0136
7	CNPO281399	40.9126
8	Annisesessine	40.6032
9	CNP0297469	37.9918
10	Vasnetine	37.0145

Furthermore, the interactions of all alkaloids with the crucial residues present at enzyme active site cavities were examined carefully in terms of classical hydrogen bond interaction, non-classical hydrogen bond interaction, hydrophobic interaction, and electrostatic interaction (**Table 3**, the 2D interaction diagrams all alkaloids with the protein M<sup>Pro</sup> were given in **Supporting Figure 2**). All the alkaloids and the reference compound famotidine were found to be involved in multiple points interactions with the residues present in M<sup>Pro</sup> active sites. Interestingly, the data in **Table 2** clearly depicts that alkaloids named CNP0368366, CNP0416047, 3-hydroxy anisotine, and Anisotine showed better or almost equal interaction energies compared to reference famotidine. Although the Anisotine was previously linked to M<sup>Pro</sup> binding (15, 16), the other three alkaloids namely CNP0368366, CNP0416047 and 3-hydroxy anisotine are entirely new leads against M<sup>Pro</sup>. Encouraged by these findings, we have chosen CNP0416047, 3-hydroxy anisotine, and anisotine as hit compounds and further examined their interaction profiles along with reference famotidine in details (**Figure 4 and Figure 5**). Regretfully, we neglected CNP0368366 from further examinations as it showed probable carcinogenicity in ADMET prediction (**Supporting Table 1**). The reference famotidine docked between the domains I and II and spanned the area between subsite S1, S1' and S4 by interacting with Asn142 (2.71Å), His163 (2.25Å), Phe140 (2.29Å), Met165(2.80Å), Arg188 (2.50Å), Glu166 (2.20Å) through conventional hydrogen bond, with Asp187 (2.75Å), Arg188 (2.75Å) via non-classical hydrogen bonds, and with active site residues His41 (4.74Å), Cys145 (5.37Å) through long-distance electrostatic interaction, but failed to provide any strong hydrogen bonding interaction with catalytic residues. The alkaloid hit CNP0416047 positioned similarly inside the catalytic cavity and showed strong conventional hydrogen bond interaction with active site residue CYS145 (2.66Å) and conserved neighbouring residue Asn142 (2.06Å), and displayed non-classical hydrogen bond and hydrophobic interactions with multiple residues interactions with Leu141 (2.58Å), His164 (3.05Å), Glu166 (2.99Å), Met165 (4.93Å), Met165 (4.93Å), Leu141 (4.80Å) along with catalytic residue His41 (4.80Å). In addition to spanning S1, S1' and S4 subsites, alkaloid CNP0416047 also covered S2 subsites through exhibiting hydrophobic interactions via its tyrosine moiety linked to C6 of quinazoline ring. The next alkaloids 3-hydroxy anisotine and anisotine showed similar interactions and covered the S1, S1' and S4 subsites of catalytic cavity. Both 3-hydroxy anisotine and anisotine exhibited strong conventional and non-classical hydrogen bonding interactions with residues present near S1 subsite such as His163, Ser144, Met165, Glu166, Phe140, and showed hydrophobic interactions with catalytic residues Cys145 and His41. Compared to anisotine, the 3-hydroxy anisotine showed one extra conventional hydrogen

bonding interaction with Gln189 (2.56Å) present at the crucial loop through the extra 3-hydroxyl group. Therefore, we have identified three natural quinazoline alkaloids namely CNP0416047, 3-hydroxy anisotine, and anisotine as hit compounds against the main protease (M<sup>Pro</sup>) of SARS\_CoV\_2 after carrying out rigid docking, pharmacokinetic analysis and flexible docking.

**Table 3:** Interaction profile of reference famotidine and selected nine alkaloids after advanced flexible docking with M<sup>Pro</sup>

Compound	Types of Interactions present with amino acids of M <sup>Pro</sup>			
	Classical Hydrogen bonding Interactions	Non classical hydrogen bonds	Hydrophobic Interactions	Electrostatics and Miscellaneous
Famotidine	Asn142 (2.71Å), His163 (2.25Å), Phe140 (2.29Å), Met165(2.80Å), Arg188 (2.50Å), Glu166 (2.20Å)	Asp187 (2.75Å), Arg188 (2.75Å)		Met165 (3.08Å), His41 (4.74Å), Cys145 (5.37Å), His172 (5.68Å)
CNP0368366	Glu166 (2.18Å, 3.00Å)	Gly143 (2.90Å), Glu166 (2.87Å), Phe140 (2.63Å), Glu166 (2.66Å)	His41 (5.88Å), His163 (5.01Å), His172 (5.01Å), Pro168 (4.67Å), Cys145 (4.30Å)	
CNP0416047	Asn142 (2.06Å), Cys145 (2.66Å)	Leu141 (2.58Å), His164 (3.05Å), Glu166 (2.99Å)	Met165 (4.93Å), His41 (4.80Å), Met165 (4.93Å), Leu141 (4.80Å)	
3-hydroxy anisotine	His163 (2.19Å), Gln189 (2.56Å), Phe140 (2.69Å)	Met165 (2.66Å), Gln189 (2.62Å), Glu166 (2.47Å), Phe140 (2.52Å),	His41 (5.09Å), Cys145 (3.71Å), His163 (3.97Å), Met165 (4.57Å), Met165 (4.63Å)	
Anisotine	Ser144 (2.96Å), His163 (2.24Å)	Glu166 (2.50Å), Glu166 (2.58Å)	Cys145 (4.39Å), Met49 (4.44Å, 5.24Å), Met165 (4.80Å), His41 (4.51Å),	Cys145 (5.70Å)
CNP0368475	Cys145 (2.34Å)	Leu141 (2.80Å), Gln189 (2.71Å)	Met49 (4.59Å), His41 (4.79Å), Met165 (4.31Å)	Cys145 (5.96Å)

Annisessine	Gly143 (2.39Å), Ser144 (2.31Å), 2.94Å), Cys145 (2.21Å)	Leu141 (2.45Å)	Glu166 (2.78Å), His41 (4.74Å), Cys145 (5.19Å), Met165 (4.44Å), Cys145 (3.99Å)	Cys145 (3.38Å)
CNP0297469	Gly143 (2.32Å), Ser144 (2.96Å), Cys145 (2.83Å)	Thr190 (2.60Å), Thr190 (2.78Å), Glu166 (2.98Å)	His41 (4.81Å), Pro168 (4.54Å), Leu27 (5.28Å), Cys145 (4.20Å)	Cys145 (3.35Å)
Vasnetine	Asn142 (2.99Å, 2.62Å), Gly143 (2.32Å), Ser144 (2.28Å, 3.00Å), Cys145 (2.15Å)	Leu141 (2.60Å), His41 (2.52Å)	His41 (4.84Å), Cys145 (4.95Å, 4.05Å), His163 (5.49Å)	Cys145 (3.32Å)

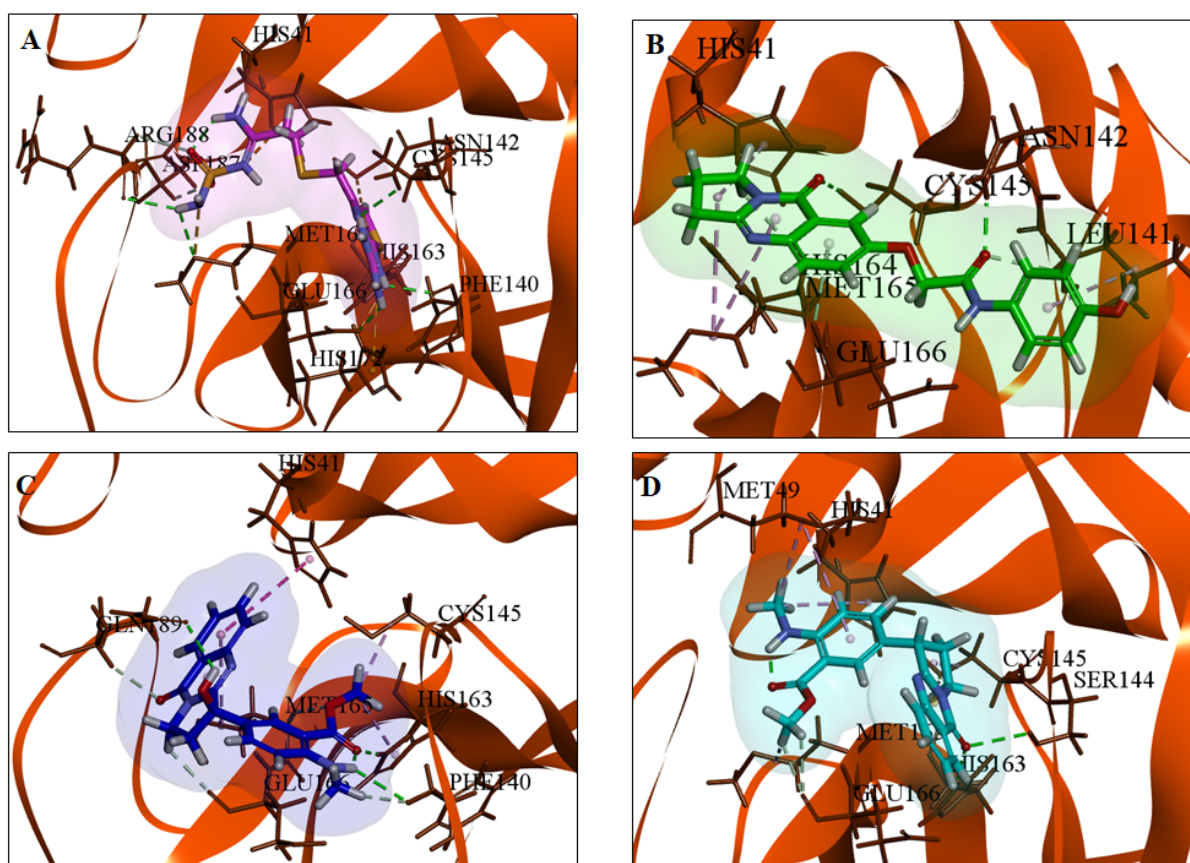


**Figure 4:** Graphical results of flexible docking studies of reference famotidine (A), and the alkaloid hits namely CNP0416047 (B), 3-hydroxy anisotine (C), and anisotine (D). The protein is represented as cartoon diagram, the interactions with amino acid residues are shown as dashed lines.

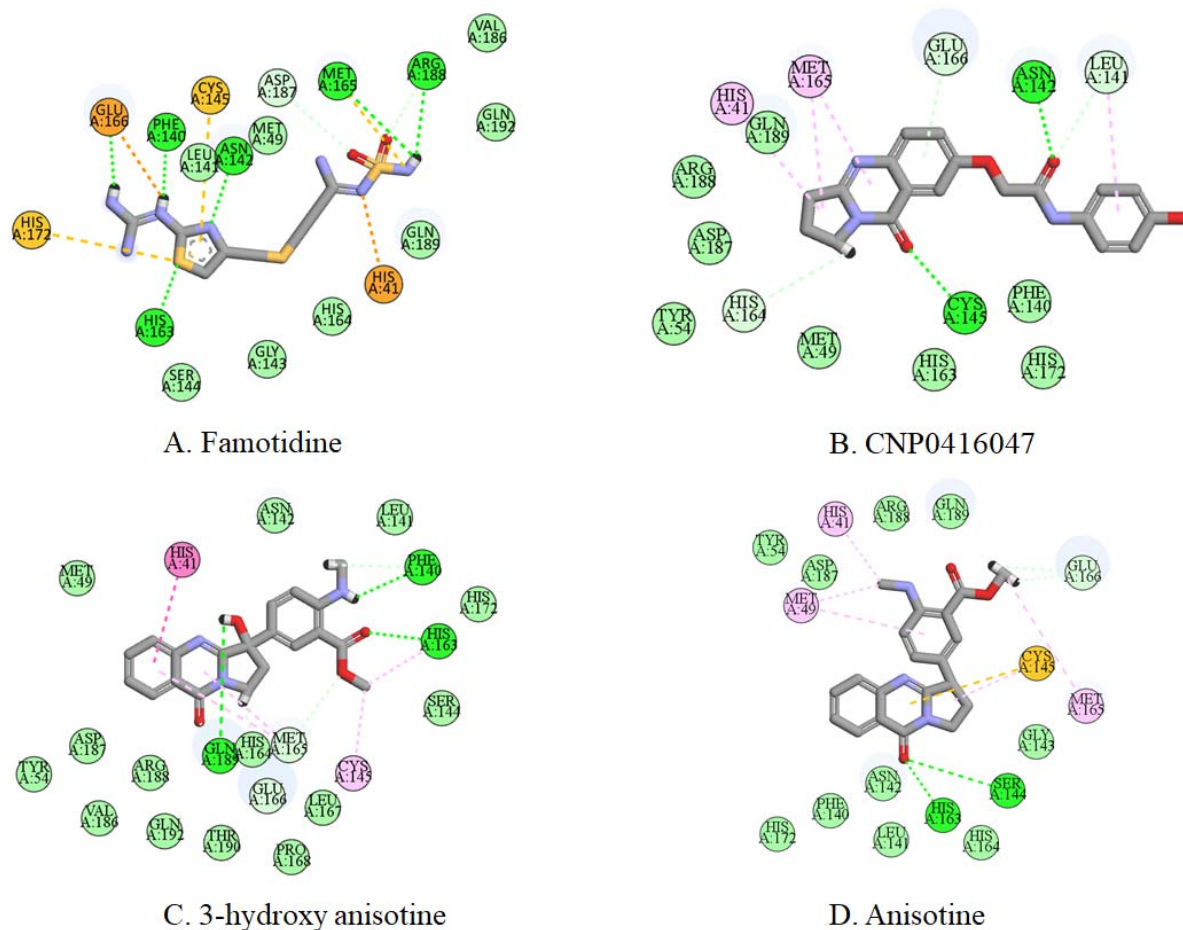


**Figure 5:** 2D interaction diagrams of reference famotidine (A), and the alkaloid hits namely CNP0416047 (B), 3-hydroxy anisotine (C), and anisotine (D).

**3.4. E-pharmacophore mapping of the hits:** E-pharmacophore hypothesis has recently emerged as a useful tool in computer-aided drug discovery and structure-based screening (38, 39, 40). In E-pharmacophore hypothesis, the combination of stereo-electronic features and energetics of a known bound ligand within the complex of its' biological target is measured computationally and later mapped with new ligands. In this study, we used E-pharmacophore model to compare the stereo-electronic features and energetics of our hit alkaloids within  $M^{Pro}$  binding site using the complex of the protein with another known non-covalent inhibitor, X77 (N-(4-tert-butylphenyl)-N-[(1R)-2-(cyclohexylamino)-2-oxo-1-(pyridin-3-yl)ethyl]-1H imidazole-4-carboxamide) (36, 37). In order to do so, the crystal structure of  $M^{Pro}$  bound with non-covalent X77 inhibitor was retrieved from RCSB database and processed as mentioned in the materials and method section to generate the energy-optimized E-pharmacophore model. As a result, total ten pharmacophores were generated having a total 12 non-bond, 4 hydrophobic and 7 hydrogen bond interactions and we selected the pharmacophore having the highest features (AAHHaromHaromHarom where A: Hydrogen bond acceptor, H: Hydrophobic, Harom: Hydrophobic aromatic respectively) for mapping our hit alkaloids (**Figure 6**). The chosen pharmacophore was then screened with alkaloid hits CNP0416047, 3-hydroxy anisotine, and anisotine respectively as one to one mapping based on a cut-off of minimum 4 features. Prior to the mapping, all three alkaloids were structurally optimized using CHARMM force field with Momary-Rone partial charge at pH 7.4 and all possible tautomers, stereoisomers and protonation states were generated. It was found that all three selected alkaloid hits were mapped to '5 features hits' indicating the hit alkaloids displayed the 5 out of 6 features in the mapping with respect to the pharmacophore.

Furthermore, the mapping was scored based on a ‘fit value’ and anisotine displayed the best fit value of 1.50884, whereas CNP0416047 mapped with lowest fit value of 0.644164 with respect to the pharmacophore.

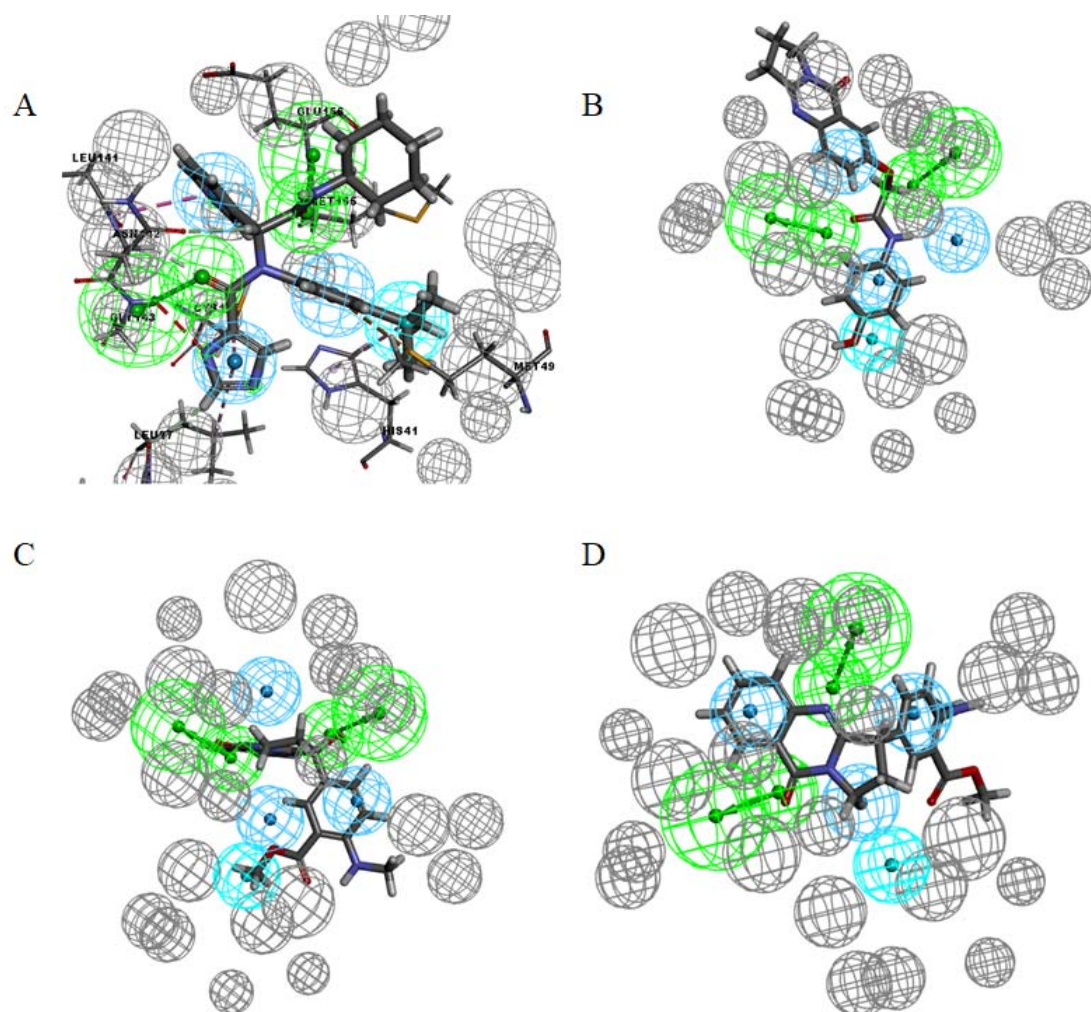


**Figure 6:** E-pharmacophore model and mapping of alkaloid hits. A. Generated E-pharmacophore model of X77 inhibitor bound inside M<sup>Pro</sup>; B. five features best hit mapping of CNP0416047 against the pharmacophore; C. Five features best hit mapping of 3-hydroxy anisotine against the pharmacophore; D. Five features best hit mapping of anisotine against the pharmacophore.

**3.5. HOMO-LUMO calculation of the hits using density functional theory:** DFT based calculation was carried out for our selected hits CNP0416047, 3-hydroxy anisotine, anisotine and for reference famotidine in order to examine the electron distribution on the frontier molecular orbitals and to calculate the HOMO-LUMO band gaps. The HOMO-LUMO energy gap has been linked to reactivity of a molecule and extrapolated to the activity of the bound inhibitor inside the enzyme catalytic cavity (28). The calculations were carried out using two different methods, B3LYP/6-311+G(D,P) (**Table 4**) and w-B97XD/6-311+G(D,P) (**Supporting Table 2**), and the independent findings of both calculations supported each other. As shown in **Table 4**, the HOMO-LUMO bandgaps of CNP0416047, 3-hydroxy anisotine and anisotine are comparable to the band gap of reference famotidine predicting that HOMO of inhibitor may smoothly transfer the electrons to the LUMO while interacting with amino acid residues at M<sup>Pro</sup> binding site. Moreover, the electron distribution at the frontier molecular orbital diagram of the hits corroborated with the findings from docking studies (**Figure 7**). The HOMO-LUMO

structures of both 3-hydroxy anisotine and anisotine displayed high electron density at the aromatic moiety attached to 3-position of tetrahydropyrrole ring showing that these aromatic moieties can exhibit strong interaction with protein residues, which supported the screening results as the alkaloids having similar structures exhibited better interaction profiles in rigid docking. Additionally, the HOMO structure of CNP0416047 has electrons localized on quinazoline frame whereas the LUMO structure has electrons on tyrosine moiety attached to C6 of quinazoline ring. From the HOMO and LUMO structures, it can be concluded that the quinazoline frame of CNP0416047 is available to donate electron to the interacting residues of the protein and in agreement with the docking results as explained in previous section.

**Table 4:** DFT based calculation using B3LYP/6-311+G(D,P) of reference famotidine and selected hits CNP0416047, 3-hydroxy anisotine, and anisotine.

COMPOUND	Energy of HOMO (a.u)	Energy of LUMO (a.u)	Band gap (ev)
Famotidine	-0.20237	-0.03887	4.4490
CNP0416047	-0.21761	-0.06181	4.2395
3-hydroxy anisotine	-0.2113	-0.05691	4.2011
Anisotine	-0.20881	-0.05595	4.1595

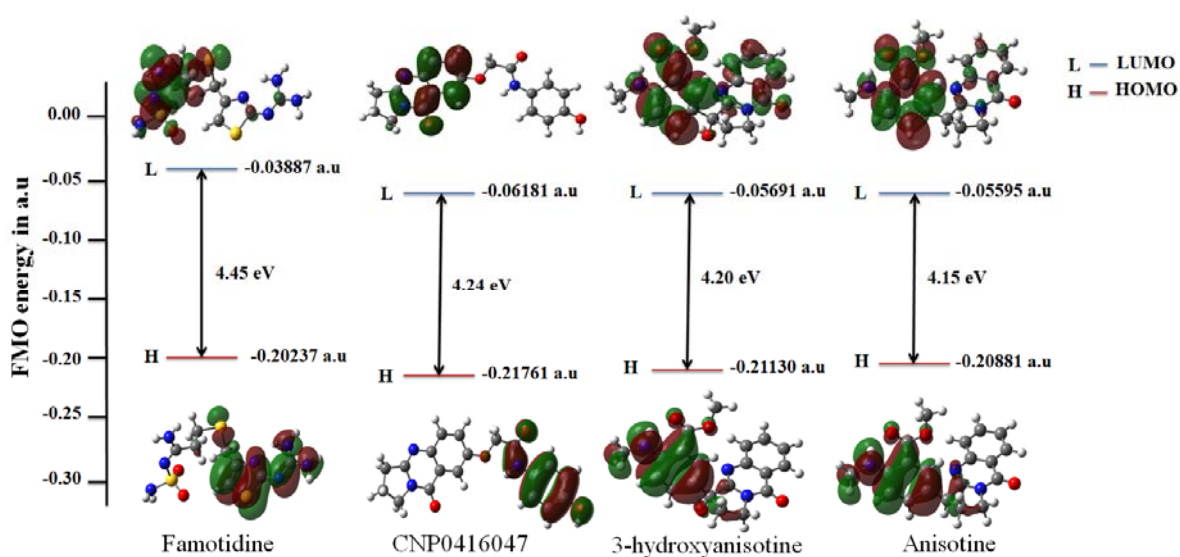


**Figure 7:** The electron distribution at the frontier molecular orbital of the hits CNP0416047, 3-hydroxy anisotine, anisotine and for reference famotidine as calculated by B3LYP/6-311+G(D,P) method.

**3.6. Molecular dynamics simulation of the hits:** The hit alkaloids CNP0416047, 3-hydroxy anisotine, and anisotine were subjected to molecular dynamics simulation along with reference famotidine to examine the conformational stability and compactness of the their complexes with the target. Purposefully, the unligated protein (only M<sup>Pro</sup>) and protein-hit complexes (M<sup>Pro</sup> – famotidine, M<sup>Pro</sup> – CNP0416047, M<sup>Pro</sup> – 3-hydroxy anisotine, and M<sup>Pro</sup> – anisotine) were simulated for 20 ns using BIOVIA Discovery Studio-Standard Dynamics Cascade program using the customized protocol as mentioned in materials and method section. In each simulation run, trajectories of 10,000 conformations were analyzed and several properties like RMSD, RMSF, radius of gyration, and binding energy were explored.

The conformational stability was evaluated by RMSD analysis by calculating the RMSD data of alpha carbon atoms of the protein backbone for all the protein-inhibitor complexes and the unligated protein with respect to the initial structures. During MD simulation the system was heated to 300 K for 120 ps at first, then equilibrated for 1 ns and then went through production phase for 20 ns beginning at 1.12 ns. The average RMSD value for M<sup>Pro</sup> protein was found to be  $0.170 \pm 0.027$  nm and for the M<sup>Pro</sup> - famotidine, M<sup>Pro</sup> -CNP0416047, M<sup>Pro</sup> -3 hydroxy anisotine, and M<sup>Pro</sup> -anisotine complexes were found to be  $0.168 \pm 0.028$ ,  $0.165 \pm 0.021$  nm,  $0.181 \pm 0.0175$ ,  $0.166 \pm 0.030$  proving the conformational stabilities of the protein-inhibitor complexes (**Table 5**). The RMSD of the native protein slightly fluctuated between 0.9 nm to 0.16 nm for the first 5 ns period of time and remained between 0.15 to 0.21 nm for the rest (**Figure 8**). The RMSD of M<sup>Pro</sup> -famotidine complex maintained a value of 0.10 - 0.15 nm up to 5 ns and reached a plateau between 0.12 nm - 0.20 nm after 5 ns with some fluctuation up to 0.26 nm at 11 ns. For M<sup>Pro</sup> -CNP0416047 complex, a plateau was reached after 5 ns with almost constant values between 0.16 nm to 0.19 nm. In case of M<sup>Pro</sup> -3 hydroxy anisotine complex, the RMSD curve became horizontal after almost 5.5 ns and the RMSD value was converged to 0.16 - 0.20 nm. The RMSD curve of M<sup>Pro</sup> -anisotine complex showed horizontal nature for first 4 ns, but fluctuate in greater extent from 5 ns to 20 ns time period than the other complexes with ranges between 0.13 nm to 0.22 nm in that period.

The fluctuation of a group of atoms and the flexibilities of different regions of protein were analyzed from RMSF calculation. In case of protein only, the higher fluctuation was observed for the Glu47 residue (0.27 nm) in domain I and for Tyr154 residue (0.24 nm) in domain II, but the rest of residues in domains I and II had low fluctuation below 0.2 nm. In the case of protein-hit complexes, the conformational fluctuation was higher at the domain III as compared to the domains I and II due to binding of the hits in between domains I and II. The average RMSF value of the native protein was found to be 0.119 nm, whether the protein-inhibitor complexes displayed lower fluctuations than M<sup>Pro</sup> displaying the stabilities of the complexes after binding (**Table 5, Figure 8**). Moreover, the detailed analysis of RMSF fluctuations of different residues and domains (I, II, III, and loop) were carried out as shown in **supplementary Table 3**. The M<sup>Pro</sup>-famotidine complex displayed higher RMSF fluctuation from 46 to 52 residue at domain I while MET49 displayed 0.48 nm RMSF value that was the highest in this region. In The M<sup>Pro</sup>-famotidine complex, domain II residues between 153 to 155 displayed RMSF value between 0.15 nm to 0.21 nm which was the highest fluctuation observed in domain II. The alkaloid CNP0416047 displayed favorable non-bonding interactions with the different residues like HIS41, HIS64, Gly143, SER144, CYS145, HIS164, GLU166, ASP187, ARG188, GLN189, GLN192, THR190, MET49, MET165, and LEU27 as evident by the low RMSF of these residues compared to the unligated M<sup>Pro</sup>. A greater fluctuation was observed in the region of 47-53 residues of domain I due to hydrophobic interaction caused by tyrosine moiety attached to C6 of quinazoline ring of CNP0416047. The 3-hydroxy anisotine interacted with the M<sup>Pro</sup> with different amino acid residues like HIS164, GLY143, ASP187, ASN142, SER144, ARG188, GLN189, THR26, LEU141, HIS41, GLU166, CYS145, CYS44, TYR54, MET165 during the entire simulation run as evident by low RMSF values compared to unligated M<sup>Pro</sup>. Different binding residues of the anisotine with M<sup>Pro</sup> during MD simulation (SER46, TYR54, GLU189, GLY143, SER144, ASN142, ARG188, HIS164, ASP187 etc.) displayed comparable RMSF to the unligated M<sup>Pro</sup>. Overall the domain II region was stabilized after the binding of inhibitors as evident by lessening of average RMSF compared to unligated M<sup>Pro</sup>.

Additionally, we calculated the radius of gyration (Rg) to measure the changes in compactness of protein molecule after the binding of inhibitors. As Rg value determines the packing of the three dimensional structure of protein molecule, therefore generally a favorable binding of ligand lowers down the Rg value. As we measured the Rg values for 20 ns simulation run of unligated M<sup>Pro</sup> and M<sup>Pro</sup>-

inhibitor complexes, it was observed that Rg for unligated M<sup>Pro</sup> was  $2.274 \pm 0.013$  nm, whether Rg for M<sup>Pro</sup>-famotidine, M<sup>Pro</sup>-CNP0416047, M<sup>Pro</sup>-3-hydroxy anisotine, M<sup>Pro</sup>-anisotine were  $2.266 \pm 0.012$  nm,  $2.274 \pm 0.011$  nm,  $2.269 \pm 0.012$  nm, and  $2.263 \pm 0.013$  nm respectively (**Table 5, Supplementary Figure 3**). Therefore, the calculated Rg values signify that the unligated protein became more compact in nature due to complexation with the inhibitor molecules and gained stabilities.

Moreover, in order to calculate the binding affinities of inhibitors towards the protein target, the molecular mechanics-Poisson-Boltzmann surface area (MM PBSA) method was carried out. For this purpose, trajectories of the simulations were processed and last 5 ns simulation data with frame increment of 250 were selected for MM PBSA calculation. The result of this calculation showed that the reference compound famotidine exhibited negative binding energy of  $19.88 \pm 0.71$  Kcal/mol, whereas alkaloid hits CNP0416047, 3-hydroxy anisotine and anisotine displayed comparable negetaive binding energies of  $22.71 \pm 0.70$  Kcal/mol,  $21.77 \pm 0.68$  Kcal/mol, and  $31.38 \pm 0.72$  Kcal/mol respectively (**Table 5**).

**Table 5:** Average RMSD, RMSF, Rg and binding energy values of unligated protein (only M<sup>Pro</sup>), reference complex (M<sup>Pro</sup> – famotidine), and protein-hit complexes (M<sup>Pro</sup> – CNP0416047, M<sup>Pro</sup> – 3-hydroxy anisotine, and M<sup>Pro</sup> – anisotine) after 20 ns simulation run.

Name of the complex	Average RMSD (nm)	Average RMSF (nm)	Average Rg (nm)	(-) Binding free energy (MM PBSA) (Kcal/mol)
M <sup>Pro</sup>	$0.170 \pm 0.027$	$0.119 \pm 0.047$	$2.274 \pm 0.013$	NA
M <sup>Pro</sup> -famotidine	$0.168 \pm 0.028$	$0.116 \pm 0.056$	$2.266 \pm 0.012$	$19.88 \pm 0.71$
M <sup>Pro</sup> - CNP0416047	$0.165 \pm 0.021$	$0.111 \pm 0.063$	$2.274 \pm 0.011$	$22.71 \pm 0.70$
M <sup>Pro</sup> -3-hydroxy anisotine	$0.181 \pm 0.017$	$0.110 \pm 0.053$	$2.269 \pm 0.012$	$21.77 \pm 0.68$
M <sup>Pro</sup> -anisotine	$0.166 \pm 0.030$	$0.118 \pm 0.058$	$2.263 \pm 0.013$	$31.38 \pm 0.72$

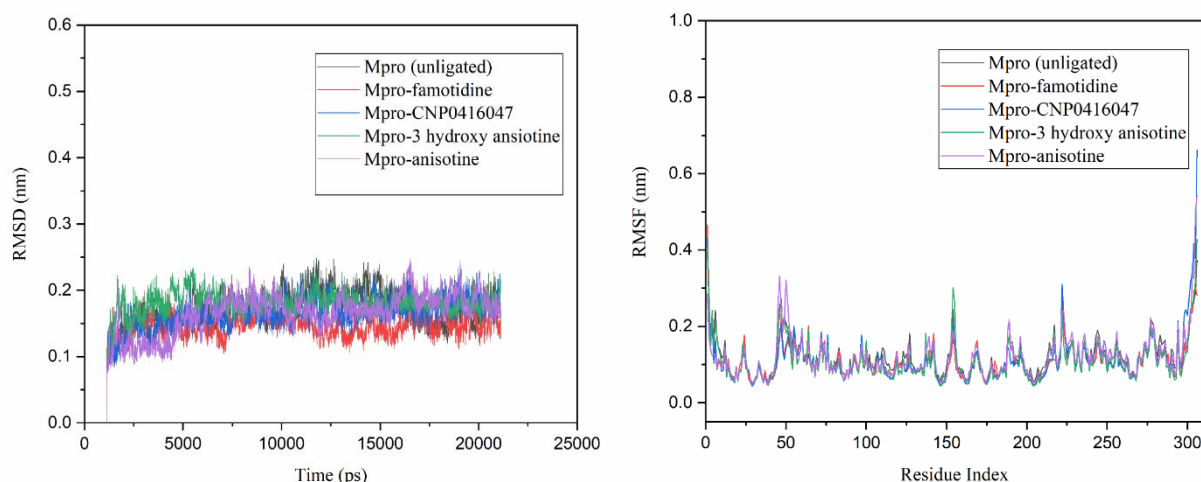


**Figure 8:** RMSD and RMSF plots of unligated protein (only M<sup>Pro</sup>), reference complex (M<sup>Pro</sup> – famotidine), and protein-hit complexes (M<sup>Pro</sup> – CNP0416047, M<sup>Pro</sup> – 3-hydroxy anisotine, and M<sup>Pro</sup> – anisotine) after 20 ns simulation run.

**4. Conclusion:** This study carried out a full-scale *in silico* investigations on natural quinazoline alkaloids against the main protease (M<sup>Pro</sup>) of SARS\_CoV\_2. This study examined 41 natural quinazoline alkaloids which are far greater in sample number compared to earlier reports and identified three alkaloids (CNP0416047, 3-hydroxy anisotine and anisotine as hit compounds. Furthermore, the structure-based binding of these hits was investigated through advanced flexible docking and E-pharmacophore mapping. Moreover, hit alkaloids were also subjected to DFT based calculation to measure the electron distribution on the frontier molecular orbitals in support of their reactivity at the binding site of M<sup>Pro</sup>. Finally, the stabilities of complexes of hit alkaloids with the protein target were accessed extensively using robust molecular dynamics simulation through RMSD, RMSF, Rg, and MM-PBSA values. Thus, this study identifies three natural quinazoline alkaloids as potential inhibitors of M<sup>Pro</sup> through extensive computational analysis. Overall, this study provides three natural quinazoline alkaloids as potential inhibitors of the main protease (M<sup>Pro</sup>) of SARS\_CoV\_2 through detailed computational methods, adds values to quinazoline pharmacophore which is a fascinating natural product and opens the possibilities of *in vitro* studies of these hit alkaloids in future.

**Acknowledgement:** DRB wants to express his gratitude to the National Institute of Technology Durgapur (NITDGP) for the platform and for providing the fund to purchase the license of BIOVIA Discovery Studio academic research suite. DRB also wants to thank Department of Chemistry (NITDGP) for the space allocated for research and acknowledges the support of Dr. Subhas Ghosal for providing HPC facilities as required for the computational studies. AJ and TR wants to thank the National Institute of Technology Durgapur (NITDGP) for the institute fellowship.

**Declaration of competing interest:** All authors declared that there is no competing interest

**Contribution:** DRB conceived the idea, carried out experiment and wrote the article. AJ carried out all experiments and assisted the paper writing. TR and SG carried out the DFT based calculations.

#### References:

1. L. Dong, S. Hu, J. Gao, discovering drugs to treat coronavirus disease 2019 (COVID-19), *Drug Discoveries & Therapeutics*, **2020**, 14, 58-60.
2. P. Forster, L. Forster, C. Renfrew, M. Forster, Phylogenetic network analysis of SARS-CoV-2 genomes, *Proc Natl Acad Sci U S A*, **2020**, 117(17), 9241-9243.
3. P. V'kovski, A. Kratzel, S. Steiner, H. Stalder, V. Thiel, Coronavirus biology and replication: implications for SARS-CoV-2, *Nature Reviews Microbiology*, **2021**, 19, 155-170.
4. Y. Huang, C. Yang, X. Xu, W. Xu, S. Liu, Structural and functional properties of SARS-CoV-2 spike protein: potential antivirus drug development for COVID-19, *Acta Pharmacologica Sinica*, **2020**, 41, 1141-1149.
5. A.R. Fehr, S. Perlman, Coronaviruses: An Overview of Their Replication and Pathogenesis, *Methods Mol Biol.*, **2015**, 128, 1-23.
6. Z. Jin, X. Du, Y. Xu, Y. Deng, M. Liu, Y. Zhao, B. Zhang, X. Li, L. Zhang, C. Peng, Y. Duan, J. Yu, L. Wang, K. Yang, F. Liu, R. Jiang, X. Yang, T. You, X. Liu, X. Yang, F. Bai, H. Liu, X. Liu, L.W. Guddat, W. Xu, G. Xiao, C. Qin, Z. Shi, H. Jiang, Z. Rao, H. Yang, Structure of Mpro from SARS-CoV-2 and discovery of its inhibitors, *Nature*, **2020**, 582, 289-293.
7. M. Kandeel, M. A. Nazawi, Virtual screening and repurposing of FDA approved drugs against COVID-19 main protease, *Life Sci.*, **2020**, 251, 117627.
8. L. Hage-Melim, L.B. Federico, N. K. S. de Oliveira, V. C. C. Francisco, L. C. Correia, H. B. de Lima, S.Q. Gomes, M.P. Barcelos, I.A.G. Francischini, C. da Silva, Virtual screening, ADME/Tox predictions and the drug repurposing concept for future use of old drugs against the COVID-19, *Life Sci.*, **2020**, 256, 117963.

9. W. Tachoua, M. Kabrine, M. Mushtaq, Z. Ul-Haq, An in-silico evaluation of COVID-19 main protease with clinically approved drugs, *Journal of molecular graphics and modelling*, **2020**, 101, 107758.
10. S. S. Gupta, A. Kumar, R. Shankar, U. Sharma, In silico approach for identifying natural lead molecules against SARS-COV-2, *Journal of molecular graphics and modelling*, **2020**, 106, 107916.
11. M. Akram, I. M. Tahir, S. M. A. Shah, Z. Mahmood, A. Altaf, K. Ahmad, N. Munir, M. Daniyal, S. Nasir, H. Mehboob, Antiviral potential of medicinal plants against HIV, HSV, influenza, hepatitis, and coxsackievirus: A systematic review, *Phytother Res.*, **2018**, 32(5), 811-822.
12. M.A. Alzohairy, Therapeutics role of *Azadirachta indica* (Neem) and their active constituents in diseases prevention and treatment, *Evid Based Complement Alternat Med.*, **2016**, 2016, 7382506.
13. R.A. Ali, M.R. Majeed, H.A. Jasmin, Determination of vasicine alkaloid efficacy as inhibitor to the activity of protease produced by a clinical isolate of *Pseudomonas aeruginosa*, *Iraqi Journal of Science*, **2018**, 59, 1237-1246.
14. S. Borkotoky, M. Banerjee, A computational prediction of SARS-CoV-2 structural protein inhibitors from *Azadirachta indica* (Neem), *J. Biomol. Struct. Dyn.*, **2021**, 39(11), 4111-4121.
15. P. Kar, V. Kumar, B. Vellingiri, A. Sen, N. Jaishee, A. Anandraj, H. Malhotra, S. Bhattacharyya, S. Mukhopadhyay, M. Kinoshita, V. Govindasamy, A. Roy, D. Naidoo, M.D. Subramaniam, Anisotine and amarogentin as promising inhibitory candidates against SARS-CoV-2 proteins: a computational investigation, *J. Biomol. Struct. Dyn.*, **2020**, 1-11
16. R. Ghosh, A. Chakraborty, A. Biswas, S. Chowdhuri, Identification of alkaloids from *Justicia adhatoda* as potent SARS CoV-2 main protease inhibitors: An in-silico perspective, *Journal of Molecular Structure*, **2021**, 1229, 129489.
17. M. Sorokina, P. Merseburger, K. Rajan, M.A. Yirik, C. Steinbeck, OCONUT online: Collection of Open Natural Products database, *Journal of Cheminformatics*, **2021**, 13, 1-13
18. T. Xu, W. Chen, J. Zhou, J. Dai, Y. Li, Y. Zhao, NPBS database: a chemical data resource with relational data between natural products and biological sources, *Database*, **2020**, 2020, baaa102
19. R. Krishnan, J.S. Binkley, R. Seeger, J. A. Pople, Self-Consistent Molecular Orbital Methods. XX. A Basis Set for Correlated Wave Functions, *J. Chem. Phys.*, **1980**, 72, 650-654
20. T. Clark, J. Chandrasekhar, G. W. Spitznagel, P. V. R. Schleyer, Efficient Diffuse Function-Augmented Basis Sets for Anion Calculations. III. The 3-21+G Basis Set for First-Row Elements, Li-F, *J. Comput. Chem.* **1983**, 4, 294-301
21. M. J. Frisch, G. W. Trucks, H. B. Schlegel, G. E. Scuseria, M. A. Robb, J. R. Cheeseman, G. Scalmani, V. Barone, G. A. Petersson, H. Nakatsuji, X. Li, M. Caricato, A. V. Marenich, J. Bloino, B. G. Janesko, R. Gomperts, B. Mennucci, H. P. Hratchian, J. V. Ortiz, A. F. Izmaylov, J. L. Sonnenberg, D. Williams-Young, F. Ding, F. Lipparini, F. Egidi, J. Goings, B. Peng, A. Petrone, T. Henderson, D. Ranasinghe, V. G. Zakrzewski, J. Gao, N. Rega, G. Zheng, W. Liang, M. Hada, M. Ehara, K. Toyota, R. Fukuda, J. Hasegawa, M. Ishida, T. Nakajima, Y. Honda, O. Kitao, H. Nakai, T. Vreven, K. Throssell, J. A. Montgomery, Jr., J. E. Peralta, F. Ogliaro, M. J. Bearpark, J. J. Heyd, E. N. Brothers, K. N. Kudin, V. N. Staroverov, T. A. Keith, R. Kobayashi, J. Normand, K. Raghavachari, A. P. Rendell, J. C. Burant, S. S. Iyengar, J. Tomasi, M. Cossi, J. M. Millam, M. Klene, C. Adamo, R. Cammi, J. W. Ochterski, R. L. Martin, K. Morokuma, O. Farkas, J. B. Foresman, and D. J. Fox, *Gaussian 16, Revision B.01*; Gaussian Inc: Wallingford CT, **2016**
22. G. M. Morris, D. S. Goodsell, R. S. Halliday, R. Huey, W. E. Hart, R. K. Belew, A. J. Olson, Automated Docking Using a Lamarckian Genetic Algorithm and an Empirical Binding Free Energy Function, *J. Computational Chemistry*, **1998**, 19(14), 1639-1662
23. A. Daina, O. Michielin, V. Zoete, SwissADME: a free web tool to evaluate pharmacokinetics, drug-likeness and medicinal chemistry friendliness of small molecules, *Sci. Rep.*, **2017**, 7, 42717
24. D. E. V. Pires, T. L. Blundell, D. B. Ascher, pkCSM: Predicting Small-Molecule Pharmacokinetic and Toxicity Properties Using Graph-Based Signatures, *J. Med. Chem.*, **2015**, 58(9), 4066-4072.

25. BIOVIA, Dassault Systèmes, BIOVIA Discovery Studio Academic Research Suite, San Diego: Dassault Systèmes, **2021**.
26. Gaussian 09 (RevisionD.01), M. J. Frisch, G. W. Trucks, H. B. Schlegel, G. E. Scuseria, M. A. Robb, J. R. Cheeseman, G. Scalmani, V. Barone, B. Mennucci, G. A. Petersson, H. Nakatsuji, M. Caricato, X. Li, H. P. Hratchian, A. F. Izmaylov, J. Bloino, G. Zheng, J. L. Sonnenberg, M. Hada, M. Ehara, K. Toyota, R. Fukuda, J. Hasegawa, M. Ishida, T. Nakajima, Y. Honda, O. Kitao, H. Nakai, T. Vreven, J. A. Montgomery Jr., J. E. Peralta, F. Ogliaro, M. J. Bearpark, J. Heyd, E. N. Brothers, K. N. Kudin, V. N. Staroverov, R. Kobayashi, J. Normand, K. Raghavachari, A. P. Rendell, J. C. Burant, S. S. Iyengar, J. Tomasi, M. Cossi, N. Rega, N. J. Millam, M. Klene, J. E. Knox, J. B. Cross, V. Bakken, C. Adamo, J. Jaramillo, R. Gomperts, R. E. Stratmann, O. Yazyev, A. J. Austin, R. Cammi, C. Pomelli, J. W. Ochterski, R. L. Martin, K. Morokuma, V. G. Zakrzewski, G. A. Voth, P. Salvador, J. J. Dannenberg, S. Dapprich, A. D. Daniels, Farkas, J. B. Foresman, J. V. Ortiz, J. Cioslowski, D. J. Fox.
27. Clark, T.; Chandrasekhar, J.; Spitznagel, G. n. W.; Schleyer, P. V. R. Efficient Diffuse Function-Augmented Basis Sets for Anion Calculations. III. The 3-21+G Basis Set for First-Row Elements, Li-F. *J. Comput. Chem.* **1983**, *4*, 294–301.
28. S. S. Mishra, S. Ranjan, C. S. Sharma, H. P. Singh, S. Kalra, N. Kumar, Computational investigation of potential inhibitors of novel coronavirus 2019 through structure-based virtual screening, molecular dynamics and density functional theory studies, *J. Biomol. Struct. Dyn.*, **2021**, 39(12), 4449-4461
29. M. Feig, C. L. Brooks III, Recent advances in the development and application of implicit solvent models in biomolecule simulations, *Current Opinion in Structural Biology*, **2004**, *14*, 217-224
30. S. Genheden, U. Ryde, The MM/PBSA and MM/GBSA methods to estimate ligand-binding affinities, *Expert Opin Drug Discov.*, **2015**, *10*(5), 449–461
31. M. Soumia, Z. Hanane, M. Benaissa, F. Z. Younes, A. Chakib, B. Mohammed, B. Mohamed, Towards potential inhibitors of COVID-19 main protease Mpro by virtual screening and molecular docking study, *J. Biomol. Struct. Dyn.*, **2020**, *14*(1), 1626-1636
32. D. E. Freedberg, J. Conigliaro, T. C. Wang, K. J. Tracey, M. V. Callahan, J. A. Abrams, Famotidine Use Is Associated with Improved Clinical Outcomes in Hospitalized COVID-19 Patients: A Propensity Score Matched Retrospective Cohort Study, *Gastroenterology*, **2020**, *159*(3), 1129–1131
33. C. Wu, Y. Liu, Y. Yang, P. Zhang, W. Zhong, Y. Wang, Q. Wang, Y. Xu, M. Li, X. Li, M. Zheng, L. Chen, H. Li, Analysis of therapeutic targets for SARS-CoV-2 and discovery of potential drugs by computational methods, *Acta Pharm Sin B.*, **2020**, *10*(5), 766-788
34. L. Shaffer, 15 drugs being tested to treat COVID-19 and how they would work, *Nat. Med.*, **2020**
35. H. R. Samimagham, M. H. Azad, M. Haddad, M. Arabi, D. Hooshyar, M. KazemiJahromi, The Efficacy of Famotidine in improvement of outcomes in Hospitalized COVID-19 Patients: A structured summary of a study protocol for a randomised controlled trial, *Trials*, **2020**, *21*, 848
36. T. Joshi, P. Sharma, T. Joshi, H. Pundir, S. Mathpal, S. Chandra, Structure-based screening of novel lichen compounds against SARS Coronavirus main protease (Mpro) as potentials inhibitors of COVID-19, *Mol. Divers.*, **2020**, 1-13
37. A. D. Mesecar, Structure of COVID-19 main protease bound to potent broad-spectrum non-covalent inhibitor X77, **2020**, doi: 10.2210/pdb6w63/pdb
38. A. Kumar, E. Rathi, S. G. Kini, E-pharmacophore modelling, virtual screening, molecular dynamics simulations and in-silico ADME analysis for identification of potential E6 inhibitors against cervical cancer, *Journal of Molecular Structure*, **2019**, *1189*, 299-306
39. K. G. Arun, C. S. Sharanya, J. Abhithaj, D. Francis, C. Sadasivan, Drug repurposing against SARS-CoV-2 using E-pharmacophore based virtual screening, molecular docking and molecular dynamics with main protease as the target, *J. Biomol. Struct. Dyn.*, **2020**, 39(13), 1-12

40. S. Jana, A. Ganeshpurkar, S. K. Singh, Multiple 3D-QSAR modeling, e-pharmacophore, molecular docking, and in vitro study to explore novel AChE inhibitors, **2018**, 8, 39477